A Modified Loading Method for Separating the Effect of Residual Stress on Fatigue Crack Growth Rate of Welded Joints

Xu, Y, Bao, R, Liu, H & Zhang, X

A Modified Loading Method for Separating the Effect of Residual Stress on Fatigue Crack Growth Rate of Welded Joints

XU Yaowu[1], BAO Rui[1*], LIU Hao[2], Xiang ZHANG[3]

[1] Institute of Solid Mechanics, Beihang University (BUAA), Beijing, 100191, P.R. China

[2] College of Aerospace Engineering, Chongqing University, Chongqing, 400044, P.R. China

[3] Faculty of Engineering, Environment and Computing, Coventry University, Coventry, CV1 5FB, UK

*Corresponding author | Email address: rbao@buaa.edu.cn

Abstract

A novel loading method is proposed to remove the effect of residual stress on measured fatigue crack growth rate in welded joint, using which the influence of empirical crack growth rate correlation equations on the results can be avoided. The total stress intensity factor range and the effective stress ratios corresponding to the combined effect of applied and residual stress are kept constant during the fatigue crack growth test, by changing the applied maximum and minimum loads with the increase of crack length and changes in residual stress based on the superposition rule. The feasibility of the proposed method was validated by tests of compact tension specimens containing residual stresses introduced by four-point bending. The loading method was then applied to a test of welded compact tension specimen with coupled effect of residual stress and microstructure change on fatigue crack growth rate. The fluctuation in the separated crack growth rate reflects the effect of microstructure change on fatigue crack growth rate.

Keywords: Fatigue crack growth, residual stress, superposition rule, weld joints

Nomenclature

a	Crack length in compact tension specimens
a_0	Initial crack length in compact tension specimens
B	Specimen thickness
C, m, n, p, q	Material constants in crack growth rate laws
D	Distance from weld centerline

E, E'	Young's modulus, Plastic modulus
$K_{app}, K_{res}, K_{tot}$	Stress intensity factor (SIF) due to applied, residual and combined stress fields
$K_{app,max}, K_{tot,max}$	SIF due to applied and combined stress fields at the maximum applied load
$K_{app,min}, K_{tot,min}$	SIF due to applied and combined stress fields at the minimum applied load
$\Delta K_{app}, \Delta K_{tot}$	SIF range due to applied and combined applied and residual stresses
$\Delta K_{app,const}$	Specified SIF range in the fatigue test
P	Externally applied load
R, R_{eff}	Applied and effective SIF ratio
$R_{eff,const}$	Specified effective SIF ratio in the fatigue test
W	Specimen width
α	Non-dimensional crack length
σ_s, σ_a	Yield strength, stress amplitude
$(da/dN)_b$	Fatigue crack growth rate (FCGR) in base material
$(da/dN)_w$	FCGR in weld metal
$(da/dN)_R$	FCGR in weld metal with residual stress effect only (no material change)
$(da/dN)_{int}$	Intrinsic FCGR in weld metal without residual stress effect

1. Introduction

The application of advanced welding technologies in metallic aircraft structures for further cost and weight savings has brought new challenges to the evaluation methods for fatigue crack growth life (FCGL) owing to the microstructural change and residual stresses, which are introduced by the welding process and demonstrate a coupled effect on fatigue crack growth rate (FCGR) [1-3]. The effect of the residual stress on FCGR will be different for different components, since the residual stress distribution is related to specimen configuration, whereas the effect of microstructural change using the same welding process will retain the same. This raises a problem when using the conventional and widely adopted approaches to evaluate the FCGL of welded joints. In these methods FCGR data obtained by laboratory specimen tests are adopted for the life prediction of components based on the theory of linear elastic fracture mechanics (LEFM). Significant amount of research has been conducted in the past 20 years to understand the crack growth behaviors in welded joints [4-13]. Some works indicate that changes in microstructure and hardness play a major role in the fusion zone or weld nugget and residual stress plays a major role outside these zones [10, 13]. Therefore,

it is a common practice that only the primary influential factor is considered in crack growth analysis of welds, e.g. residual stress plays a major role on the FCGR for crack propagation perpendicular to a weld, consequently, the superposition rule is adopted in this case to account for the combined effects of residual and applied stresses on crack growth. Microstructural change effect, although presents obviously in weld nugget, is ignored [6]. For improvement of the accuracy of crack growth life prediction of welds, Zhang and Bao [3] proposed the method of superposing the effect of residual stress on the intrinsic crack growth rate (ICGR) of weld metal rather than on the FCGR of the base metal. ICGR is related to microstructural change and can be obtained by separating the contribution of residual stress from the measured FCGRs of welded laboratory specimens; the remaining crack growth rate change is attributed to the contribution from the microstructural changes in the weld metal. No matter whether to superpose the residual stress effect on the base material FCGR or on the weld ICGR, using different crack growth rate equation will result in difference in the predicted residual stress effect, which will be illustrated in detail in the next section. Some researchers proposed methods to relieve the residual stress in welds, e.g. by applying a 2% positive plastic strain along the welding centerline, to obtain the FCGR with only the effect of microstructural change [12, 13]. However, different conclusions were obtained on the crack growth behavior inside weld in [12] and [13], although the same residual stress relief method was used for the same friction stir welded 2024-T351 aluminum. Furthermore, the welding-induced residual stress could not be entirely released by the aforementioned mechanical approach, and eventually, about 10% of the original stress was remained. Changes in the weld metal microstructure and properties during plastic stretching also seem to be inevitable.

A novel FCGR test method, by which the effect of residual stress on FCGR can be removed via changing the applied load, is proposed in this paper. Although this method is still based on the superposition rule, the influence of empirical FCGR correlation equations on the results is avoided, because the separation of residual stress effect on FCGR is carried out when determining the applied loads in the test rather than until dealing with the final measured FCGR data. Two case studies were carried out to demonstrate the applicability of the proposed method. One of them is the fatigue crack propagation test using specimens containing only residual stresses and negligible microstructural changes (residual stress was introduced by four-point bending load), and the other is the fatigue crack propagation test with friction stir welded [14] specimens having both residual stress and microstructural change effects on FCGR. Based on the test results of the welded specimen, the changes in FCGR in different weld zones are also discussed.

2. Problem in Separating Residual Stress Effect using Empirical FCGR Correlation Equations

FCGR of welded joints could be correlated or predicted by adding the effect of residual stress on FCGR to the crack growth rate of the base material [5, 6], Eq. 1, or to the ICGR of weld [3], Eq. 2.

$$\left(\frac{\mathrm{d}a}{\mathrm{d}N}\right)_{\mathrm{w}} = \left(\frac{\mathrm{d}a}{\mathrm{d}N}\right)_{\mathrm{b}} + \Delta_1 = \left(\frac{\mathrm{d}a}{\mathrm{d}N}\right)_{\mathrm{R}} \tag{1}$$

$$\left(\frac{\mathrm{d}a}{\mathrm{d}N}\right)_{\mathrm{w}} = \left(\frac{\mathrm{d}a}{\mathrm{d}N}\right)_{\mathrm{b}} + \Delta_1 + \Delta_2 = \left(\frac{\mathrm{d}a}{\mathrm{d}N}\right)_{\mathrm{int}} + \Delta_1 = \left(\frac{\mathrm{d}a}{\mathrm{d}N}\right)_{\mathrm{R}} + \Delta_2 \tag{2}$$

where $(\mathrm{d}a/\mathrm{d}N)_{\mathrm{w}}$ and $(\mathrm{d}a/\mathrm{d}N)_{\mathrm{b}}$ represent the FCGRs of welded specimens and base materials, respectively. Term $(\mathrm{d}a/\mathrm{d}N)_{\mathrm{R}}$ is the FCGR in weld metal with only the effect of residual stress (no material change), while $(\mathrm{d}a/\mathrm{d}N)_{\mathrm{int}}$ is the weld ICGR which contains only the effect of microstructural changes. Therefore, Δ_1 represents the effect of residual stress on FCGR and Δ_2 means the effect of microstructural changes on FCGR. Both $(\mathrm{d}a/\mathrm{d}N)_{\mathrm{w}}$ and $(\mathrm{d}a/\mathrm{d}N)_{\mathrm{b}}$ can be obtained by fatigue crack propagation tests and $(\mathrm{d}a/\mathrm{d}N)_{\mathrm{R}}$ can be calculated by the empirical laws. However, different FCGR laws usually result in discrepancies in predictions of $(\mathrm{d}a/\mathrm{d}N)_{\mathrm{R}}$. This means that the prediction of $(\mathrm{d}a/\mathrm{d}N)_{\mathrm{w}}$ will be influenced by the chosen empirical law, and moreover, the identification of the effect of microstructural change on FCGR will also be affected when the contribution of residual stress to FCGR is separated using Eq. (2). Hence, a method for removing the effect of residual stress on FCGR, which is independent of the correlation equations, is presented by this study.

Due to the availability of residual stress and for the convenience of further analyses, a welded middle-crack tension (MT) specimen in [3] is used as a demonstration example for evaluating $(\mathrm{d}a/\mathrm{d}N)_{\mathrm{R}}$. The specimen is made of aluminum alloy 2024-T351 and contains a central weld created by the Variable Polarity Plasma Arc (VPPA) welding technique [15]. The specimen has a dimension of 80 mm × 360 mm and a thickness of 7 mm. Measured longitudinal residual stresses and corresponding stress intensity factors (SIFs) are shown in Fig. 1. The SIFs of the residual stress (K_{res}) are calculated using the displacement extrapolation method in the ANSYS software using the command "KCALC" in the general postprocessor after defining the path for extracting the crack region displacements. Procedures of the finite element (FE) analysis for the K_{res} determination are detailed in [16].

The commonly used crack growth rate laws, such as the equations proposed by Walker (Eq. (3)) [17] and Forman (Eq. (4)) [18], and the NASGRO equation (Eq. (5)) [19] are used here to correlate the FCGR.

$$\frac{\mathrm{d}a}{\mathrm{d}N} = C\left[\Delta K\left(1-R\right)^{m-1}\right]^{n} \tag{3}$$

$$\frac{\mathrm{d}a}{\mathrm{d}N} = \frac{C\left(\Delta K\right)^{n}}{K_{\mathrm{crit}}\left(1-R\right)-\Delta K} \tag{4}$$

$$\frac{\mathrm{d}a}{\mathrm{d}N} = C\left[\left(\frac{1-f}{1-R}\right)\Delta K\right]^{n}\frac{\left(1-\dfrac{\Delta K_{\mathrm{th}}}{\Delta K}\right)^{p}}{\left(1-\dfrac{K_{\mathrm{max}}}{K_{\mathrm{crit}}}\right)^{q}} \tag{5}$$

where C, m, n, p, q, K_{crit}, ΔK_{th} are all material constants, f is a parameter correlating with the stress ratio R. In the presence of residual stresses, the superposition method presented by Glinka and Parker [20, 21], which is based on the principle of LEFM, is used to consider the effect of residual stresses on the FCGRs. In this condition, the SIF range ΔK and the stress ratio R are replaced by the total SIF range ΔK_{tot} and the effective SIF ratio R_{eff}, respectively, which are given as Eqs. (6) and (7).

$$\Delta K_{\mathrm{tot}} = K_{\mathrm{tot,max}} - K_{\mathrm{tot,min}} = \left(K_{\mathrm{app,max}} + K_{\mathrm{res}}\right) - \left(K_{\mathrm{app,min}} + K_{\mathrm{res}}\right) = \Delta K_{\mathrm{app}} \tag{6}$$

$$R_{\mathrm{eff}} = \frac{K_{\mathrm{app,min}} + K_{\mathrm{res}}}{K_{\mathrm{app,max}} + K_{\mathrm{res}}} \tag{7}$$

Two loading conditions are considered for evaluating $(\mathrm{d}a/\mathrm{d}N)_{\mathrm{R}}$: constant amplitude (σ_{a}) loading and constant ΔK_{app} loading, as shown in Table 1. Material constants used in the Walker, Forman and NASGRO equations are summarized in Table 2. Evaluated $(\mathrm{d}a/\mathrm{d}N)_{\mathrm{R}}$ and $(\mathrm{d}a/\mathrm{d}N)_{\mathrm{b}}$ are shown in Figs. 2(a) and (b).

For $(\mathrm{d}a/\mathrm{d}N)_{\mathrm{b}}$ in the constant amplitude (CA) load condition, the Walker and NASGRO predictions agree well with each other when $a < 12$ mm and the difference between them starts to widen as $a > 12$ mm, whereas difference between the Forman and NASGRO predictions is reduced with the increase of the crack length. The reason is that both the Forman and NASGRO equations take account of the final and fast crack growth stage when K_{max} approaches K_{crit}, but the Walker equation does not. However, for $(\mathrm{d}a/\mathrm{d}N)_{\mathrm{R}}$ in the CA loading case, differences among the Walker, Forman and NASGRO predictions are much greater compared with those in $(\mathrm{d}a/\mathrm{d}N)_{\mathrm{b}}$. For the constant ΔK_{app} (CK) load condition, $(\mathrm{d}a/\mathrm{d}N)_{\mathrm{b}}$ predicted by all equations are constant and only small differences are observed in the predictions. The trends of $(\mathrm{d}a/\mathrm{d}N)_{\mathrm{R}}$ evaluations are similar to that of the K_{res} distribution, and the Walker and Forman predictions agree well when $a < 15$ mm or $a > 25$ mm, but discrepancies in magnitude between Walker (or Forman) and NASGRO predictions are significant.

In conclusion, although similar evaluations for $(\mathrm{d}a/\mathrm{d}N)_{\mathrm{b}}$ were provided by the correlation equations, greater discrepancies appear in the predictions of $(\mathrm{d}a/\mathrm{d}N)_{\mathrm{R}}$, i.e. the sensitivity of residual stress for $(\mathrm{d}a/\mathrm{d}N)_{\mathrm{R}}$ varies with the selection of the empirical crack growth law.

3. Proposal of a Modified Loading Method for Removing the Effects of Residual Stress

The established FCGR laws, such as the Walker and Forman equations, indicate that FCGR is governed by the SIF range ΔK and the SIF ratio R. In the presence of residual stress, the superposition model demonstrates that the total SIF range ΔK_{tot} remains the same as the applied one, and only the effective SIF ratio R_{eff} responds to the residual stress according to Eqs. (6) and (7). If R_{eff} can be kept constant during the fatigue test by controlling the externally applied loads, then the effect of residual stress on the FCGR can be removed. Therefore, fatigue crack propagation tests can be performed in CA or CK loading condition using a constant SIF ratio ($R_{eff,const}$) to separate the contribution of the residual stress. To reflect the influence of microstructural changes on FCGR in different zones, a constant crack growth driving force (SIF range and R_{eff}) was maintained during the tests, i.e. a CK loading condition was employed in this study taking account of the residual stress variation with the growing crack length. Based on Eqs. (8) and (9), the applied SIF K_{app} can be calculated as:

$$K_{app,max} = \frac{\Delta K_{app,const}}{1 - R_{eff,const}} - K_{res} \tag{8}$$

$$K_{app,min} = \frac{\Delta K_{app,const}}{1 - R_{eff,const}} - K_{res} - \Delta K_{app,const} \tag{9}$$

According to the LEFM theory, the stress intensity factor K is a function of externally applied loads P and crack length a. Considering the problems of using MT specimens for investigating the FCGR in weld zones, compact tension (CT) specimens were selected in this study. The applied load with respect to crack length can be calculated by Eq. (10) from ASTM E647-11 [23]:

$$P = K_{app} B \sqrt{W} \frac{(1-\alpha)^{3/2}}{(2+\alpha)} \left(0.886 + 4.64\alpha - 13.32\alpha^2 + 14.72\alpha^3 - 5.6\alpha^4 \right)^{-1} \tag{10}$$

where $\alpha = a/W$.

A flowchart of the proposed method and calculation procedure is shown in Fig. 3.

4. Case Studies with the Proposed Loading Method

4.1. FCGR in CT specimens with only residual stress introduced by four-point bending load

First, the presented loading method should be verified to show that the effect of residual stress on FCGR can be removed during the fatigue tests. CT specimens were prepared with residual stresses being introduced by four-point bending load. Microstructural change introduced by the plastic deformation was negligible compared with that induced by welding process.

4.1.1. Specimen preparation

The CT specimens, denoted as CT_{4PB}-1, 2 and CT_{4PB}-3, 4, were extracted from beam specimens after four-point bending load to plastic deformation, as shown in Fig. 4. The beam was made of aluminum alloy plate 2024-T351 with a cross-section dimension of 10 mm × 50 mm and a length of 320 mm. The four-point bending fixture was arranged such that the distance between the outer contact pins was 300 mm, and the distance between the inner pins was 120 mm. Then the beam was slowly loaded to a maximum load of 41 kN. Residual stresses in specimens CT_{4PB}-1, 2 and CT_{4PB}-3, 4 had the opposite distribution trend along the crack growth direction (Fig. 5). Two further CT specimens without residual stresses (denoted as CT_{BM}-1 and CT_{BM}-2) were also prepared for the comparison.

The CT specimen dimensions were in accordance with ASTM E647-11: width $W = 40$ mm, thickness $B = 10$ mm and initial notch length $a_0 = 8$ mm.

4.1.2. Residual stress and K_{res}

An elasto-plastic FE simulation of the four-point bending process was performed with the ANSYS package to obtain the longitudinal residual stress distribution along the width of the specimen. The material constants in the bilinear model were obtained by static tensile tests, finding the Young's modulus $E = 72.5$ GPa, plastic modulus $E' = 6$ GPa and yield strength $\sigma_s = 291$ MPa. Subsequently, K_{res} due to the given residual stress field was calculated using the displacement extrapolation method. The residual stress distribution and corresponding K_{res} of specimens CT_{4PB}-1, 2 and CT_{4PB}-3, 4 are presented in Fig. 5. Both the residual stress and K_{res} distributions have the opposite trend in the two kinds of specimens owing to the different crack location.

During the bending process, longitudinal strain in the central part of the beam specimen was monitored using the digital image correlation technique. The data were shown to be highly consistent with the analysis results from the FE simulations and the deviation of the maximum strain value was less than 5%, which has convinced us that the residual stress profile derived by FE simulation is the actual stress distribution in the beam.

4.1.3. Fatigue crack propagation tests

Fatigue crack propagation tests were conducted at 20 Hz load frequency using a MTS servo-hydraulic fatigue test machine with a 10 kN load cell; the loading conditions are summarized in Table 3. The crack length was monitored from the specimen surface by a traveling microscope, and the externally applied load P with respect to the crack length was obtained using Eq. (10). Changes in the applied P_{max} and P_{min} with the

increasing crack length are given in Fig. 6 for the two kinds of specimens in order to achieve constant R_{eff} and constant ΔK_{app}.

4.1.4. Results and discussion

Fatigue crack growth rate of the specimens with different residual stresses were investigated in three different cases, i.e. $K_{res} > 0$, $K_{res} < 0$ and $K_{res} = 0$ in the crack growth regime. Fig. 7(a) shows the comparison of FCGRs between CT_{4PB}-1, 2 ($K_{res} > 0$) and CT_{BM}-1 ($K_{res} = 0$) in the case of $R_{eff, const} = 0.5$, whereas the FCGRs of CT_{4PB}-3, 4 ($K_{res} < 0$) and CT_{BM}-2 ($K_{res} = 0$) in the case of $R_{eff, const} = 0.1$ are shown in Fig. 7(b). These data were obtained using the secant method. They were then compared to the average FCGRs of the CT_{BM} specimens.

In the case of $K_{res} > 0$, FCGRs of CT_{4PB}-1, 2 remained substantially unchanged; FCGRs were mainly distributed in the range of $(1.2 \sim 2.3) \times 10^{-4}$ mm/cycle and slightly fluctuated in the vicinity of the average value 2.28×10^{-4} mm/cycle (CT_{BM}-1). While a similar situation was observed in the case of $K_{res} < 0$, FCGRs of CT_{4PB}-3, 4 approximately located in the $(1.1 \sim 2.1) \times 10^{-4}$ mm/cycle and fluctuated near the average value 1.15×10^{-4} mm/cycle (CT_{BM}-2). In summary, FCGRs in CT_{4PB}-1, 2 and CT_{4PB}-3, 4 corresponded with the FCGRs in CT_{BM}-1 and CT_{BM}-2, in which $K_{res} = 0$, respectively. This result means that FCGR can be identical if the tests were performed with a constant ΔK_{app} and constant R_{eff}, regardless of the presence of residual stresses, i.e. the effect of residual stress on FCGR can be removed by this proposed modified loading method.

4.2. FCGR in friction stir welded CT specimen

4.2.1. Specimen preparation

The 2024-T351 alloy was supplied as plate with a thickness of 5 mm. Two parent metal plates of 500 mm × 250 mm were friction stir welded along their long edge and parallel to the rolling (L) orientation. The welding tool used in this study had a shoulder of 12 mm diameter; measured process parameters were a rotation rate of 600 rpm and a traverse speed of 100 mm/min.

After being butt welded by friction stir welding (FSW), the plates were cut into a strip of 65 mm × 300 mm size, as shown in Fig. 8, to measure the longitudinal residual stress introduced by the welding process using the contour method originally proposed by Prime [24]. The strip was carefully cut into two pieces along a transverse plane, and the vertical (longitudinal) displacement profile of the cutting surface caused by the release of residual stress was measured. Then, the opposite of the measured displacement profile was applied as boundary conditions to the surface of an FE model and the corresponding longitudinal residual stress distribution was obtained.

CT specimens with nominal crack growth in the direction perpendicular to the weld centerline were cut from the strip and specified as CT_{FSW}-1, 2; the specimen geometry shown in Fig. 8 was established in accordance with ASTM E647-11: W = 52 mm, B = 5 mm and a_0 = 10.4 mm. Another specimen of identical dimension was manufactured from the base material, denoted as CT_{BM}-3, for comparison purpose.

4.2.2. Residual stress and K_{res}

Measured residual stress profile and calculated K_{res} by the displacement extrapolation method are shown in Fig. 9. Residual stresses in the weld zone were tensile with the external regions being subjected to compressive residual stresses. Two peaks were located 5 mm from the weld centerline on both sides, and a valley stress located at the weld centerline between the two maxima. The maximum stress, which occurred on the advancing side, was 44% of the parent plate (L) yield strength. The trend of the residual stress distributions obtained in this study compared well with other published results of FSW residual stresses [13, 25]. Although there is a difference in the maximum stress value between the advancing and the retreating side, the distribution is nearly symmetric about the weld centerline. Thus, the side, from which the fatigue crack starts to propagate, should not significantly affect the result. Therefore, crack propagation test was performed with the crack propagating from the FSW retreating side to the advancing side.

4.2.3. Fatigue crack growth tests

Fatigue test details are similar to that described in Section 4.1.3 and the loading conditions are summarized in Table 4.

4.2.4. Results

Fig. 10 shows the crack growth rate curves for CT_{FSW}-1, 2 and the base material specimen CT_{BM}-3. As expected, FCGR of CT_{BM}-3 remained steady at approximately the average value 1.78×10^{-4} mm/cycle. Considerable fluctuations were shown in the FCGR of the CT_{FSW} specimens: from the retreating side, FCGR decreased as the crack approached the weld reaching a minimum FCGR (~5×10^{-5} mm/cycle) at approximately 3 mm from the weld centerline. Then it began to rebound and recovered to a level similar to that of CT_{BM}-3. Subsequently, the crack propagated into the advancing side and the FCGR decreased again after the crack tip had passed the weld centerline. A second minimum FCGR of ~6×10^{-6} mm/cycle was attained approximately 8 mm from the weld centerline, after which the FCGR rapidly increased and stabilized at the base material level. Based on the similitude principle that FCGR should be the same if the crack propagation tests were performed with constant ΔK_{app} and R_{eff}, which was presented in Section 4.1, the discrepancy between the FCGRs of CT_{BM}-3 and CT_{FSW} specimens was attributed to the microstructure

change introduced by the welding process.

4.2.5. Discussion on the crack growth rate fluctuation in CT$_{FSW}$ specimen

For better understanding of the fluctuation shown in Fig. 10 in the CT$_{FSW}$ specimens under the constant ΔK and constant R_{eff} loading, changes in microstructure, hardness and static mechanical properties were measured.

The microstructure changes were observed on a polished and etched specimen (Keller's reagent: 1 mL HF, 1.5 mL HCl, 2.5 mL HNO$_3$ and 95 mL H$_2$O), as shown in Fig. 11. Three different zones appeared after the FSW process due to intense plastic deformation and high-temperature exposure within and around the stirred area; they were identified as the weld nugget zone (WNZ), the thermo-mechanically affected zone (TMAZ), and the heat-affected zone (HAZ) based on the microstructural characterization; the approximate sizes of these zones are: WNZ ($D < 3$ mm), TMAZ ($3 < D < 6$ mm), HAZ ($6 < D < 8$ mm), and BM ($D > 8$ mm), where D is the distance from the weld centerline.

The Vickers Hardness distribution across the friction stir welded joint was determined in different layers and compared to the hardness of the base material (145 HV), as shown in Fig. 12. The HV test load was 0.1 kg. The weld zone has a relatively low hardness than the base material, and the hardness in the vicinity of the weld centerline presented a downward trend from the top surface to the bottom surface. The hardness recovered to a level similar to that of the base material immediately outside the weld at approximately 8 mm from the weld centerline, which revealed the range of the heat affected zones. The hardness distribution seemed to be symmetric and the difference between the retreating side and the advancing side was minimal.

The local static mechanical properties in different zones were evaluated by tensile tests and compared with the base material in Fig. 13. Similarities among the profiles of yield strength, ultimate tension strength (UTS) and elongation are as follows: Two minima were located 5 mm from the weld centerline, and the values recovered to the level of the base material once outside the weld. However, distinct discrepancies also existed among the distributions: The yield strength almost approached the base material value in the vicinity of the weld centerline, and only minor distinctions was presented between the retreating side and the advancing side. While the UTS and elongation distribution exhibited a valley at the weld centerline and considerable differences between the both sides.

From the investigation of changes in the microstructure, hardness and mechanical properties, the fluctuation in FCGR of the CT$_{FSW}$ specimens shown in Fig. 10 is the result of the material characteristic changes in different weld zones:

(1) WNZ. The variation of the FCGR might be explained as follows: The weld metal in the WNZ was softer than the base metal, and the grain size in this region was much smaller than that of the base material. They both cause a lower FCGR. However, the lower elongation at the weld centerline resulted in poor ductility and consequently enabled the FCGRs at the weld centerline to attain the level of the base material.

(2) TMAZ and HAZ. The variations of the FCGRs in the TMAZ and HAZ were more complicated due to the unsymmetrical profile about the weld centerline. On the retreating side, the reduction of FCGR from HAZ to TMAZ was induced partly by the lower hardness and partly by the lower yield strength. This is because that the lower hardness can make the weld metal much softer, and lower yield strength results in a larger crack tip plastic zone. Moreover, the FCGR was also influenced by the elongation and the microstructural changes: the minimum FCGR was located 3 mm from the weld centerline, where the elongation has reached its peak value and the boundary between the TMAZ and the WNZ was located exactly at this position. Both high ductility and fine grain size produce a lower FCGR. On the advancing side, similarly, the reduction in FCGRs was caused by the softer metal and larger crack tip plastic zone, which were resulted from the lower hardness and yield strength in this region.

5. Conclusions

(1) The proposed loading method for separating the effects of residual stress on FCGR during the tests are simple and feasible to use to avoid the influence of empirical crack growth rate correlation equations on the calculated result according to the basic idea of the method.

(2) Test results of CT specimens containing residual stresses introduced by four-point bending demonstrate the validity of the proposed method in both cases of $K_{res} > 0$ and $K_{res} < 0$ for removing the effect of residual stress on FCGR.

(3) Test result of friction stir welded 2024-T351 specimens has demonstrated the applicability of the proposed method to isolate the contributions of residual stress and microstructure change to FCGR in weld parts. The changes in microstructure, hardness and mechanical properties in different weld zones account for the observed fluctuations in the FCGR that is free from the residual stress effect as obtained by the proposed method.

References

[1]. Schmidt HJ (2005, June). Damage tolerance technology for current and future aircraft structures. In *Proceedings of the 23rd ICAF Symposium of the international Committee on Aeronautical Fatigue* (Vol. 1, pp. 1-41).

[2]. Zhang X, Irving P, Edwards L, Fitzpatrick M, Sinclair I, Lin J, Yapp D (2005, June). The influence of residual stress on design and damage tolerance of welded aircraft structures. In *Proceedings of the 23rd ICAF Symposium of the International Committee on Aeronautical Fatigue* (Vol. 1, pp. 265-281).

[3]. Zhang X, Bao R (2011). Evaluation of the intrinsic crack growth rates of weld joints. *Int. J. Fatigue*, 33(4), 588-596.

[4]. Božić Ž, Schmauder S, Mlikota M, Hummel M (2014). Multiscale fatigue crack growth modelling for welded stiffened panels. *Fatigue Fract. Eng. Mater. Struct.*, 37(9), 1043-1054.

[5]. Ghidini T, Donne CD (2007). Fatigue crack propagation assessment based on residual stresses obtained through cut-compliance technique. *Fatigue Fract. Eng. Mater. Struct.*, 30(3), 214-222.

[6]. Servetti G, Zhang X (2009). Predicting fatigue crack growth rate in a welded butt joint: The role of effective R ratio in accounting for residual stress effect. *Eng. Fract. Mech.*, 76(11), 1589-1602.

[7]. Sutton MA, Reynolds AP, Ge YZ, Deng X (2006). Limited weld residual stress measurements in fatigue crack propagation: Part II. FEM-based fatigue crack propagation with complete residual stress fields. *Fatigue Fract. Eng. Mater. Struct.*, 29(7), 537-545.

[8]. Milan MT, Bose Filho WW, Ruckert COFT, Tarpani JR (2008). Fatigue behaviour of friction stir welded AA2024‐T3 alloy: longitudinal and transverse crack growth. *Fatigue Fract. Eng. Mater. Struct.*, 31(7), 526-538.

[9]. Vaidya WV, Staron P, Horstmann M (2012). Fatigue crack propagation into the residual stress field along and perpendicular to laser beam butt-weld in aluminium alloy AA6056. *Fatigue Fract. Eng. Mater. Struct.*, 35(5), 399-411.

[10]. Tra TH, Okazaki M, Suzuki K (2012). Fatigue crack propagation behavior in friction stir welding of AA6063-T5: Roles of residual stress and microstructure. *Int. J. Fatigue*, 43, 23-29.

[11]. Pouget G, Reynolds AP (2008). Residual stress and microstructure effects on fatigue crack growth in AA2050 friction stir welds. *Int. J. Fatigue*, 30(3), 463-472.

[12]. Bussu G, Irving PE (2003). The role of residual stress and heat affected zone properties on fatigue crack propagation in friction stir welded 2024-T351 aluminium joints. *Int. J. Fatigue*, 25(1), 77-88.

[13]. Fratini L, Pasta S, Reynolds AP (2009). Fatigue crack growth in 2024-T351 friction stir welded joints: Longitudinal residual stress and microstructural effects. *Int. J. Fatigue*, 31(3), 495-500.

[14]. Mishra RS, Ma ZY (2005). Friction stir welding and processing. *Mater. Sci. Eng. R*, 50(1), 1-78.

[15]. Hou R, Evans DM, McClure JC, Nunes AC, Garcia G (1996). Shielding gas and heat transfer efficiency in plasma arc welding. *Weld J.*, 75(10), 305-310.

[16]. Bao R, Zhang X, Yahaya NA (2010). Evaluating stress intensity factors due to weld residual stresses by the weight function and finite element methods. *Eng. Fract. Mech.*, 77(13), 2550-2566.

[17]. Walker K (1970). The effect of stress ratio during crack propagation and fatigue for 2024-T3 and 7075-T6 aluminum. In *Effects of environment and complex load history on fatigue life*. ASTM International.

[18]. Forman RG, Kearney VE, Engle RM (1967). Numerical analysis of crack propagation in cyclic-loaded structures. *J. Basic Eng.*, 89(3), 459-63.

[19]. Harter JA. AFGROW users guide and technical manual, AFRL-VA-WP-TR-2006-XXXX, AFGROW for Windows 2K/XP, Version 4.0011.14; June 2006. http://www.siresearch.info/projects/afgrow/downloads/afgrow/ddownload.php [Accessed July 2008].

[20]. Glinka G (1979, January). Effect of residual stresses on fatigue crack growth in steel weldments under constant and variable amplitude loads. In *Fracture Mechanics: Proceedings of the Eleventh National Symposium on Fracture Mechanics: Part I*. ASTM International.

[21]. Parker AP (1982). Stress intensity factors, crack profiles, and fatigue crack growth rates in residual stress fields. In *Residual stress effects in fatigue*. ASTM International.

[22]. Kumar A, MURTHY R, Iyer NR (2013). A study of the stress ratio effects on fatigue crack growth using LOWESS regression. In *International Conference on Advances in Civil, Structural and Mechanical Engineering–CSM* (pp. 47-51).

[23]. ASTM International (2011). *Standard test method for measurement of fatigue crack growth rates*. ASTM International.

[24]. Prime MB, Gonzales AR (2000, July). The contour method: simple 2-D mapping of residual stresses. In *Proceedings of the 6th International Conference on Residual Stresses*, Oxford, UK (Vol. 1, pp. 617-24). Livermore Software Technology.

[25]. Staron P, Kocak M, Williams S, Wescott A (2004). Residual stress in friction stir-welded Al sheets. *Physica B: Condensed Matter*, 350(1), E491-E493.

Table 1. Loading conditions for $(\mathrm{d}a/\mathrm{d}N)_R$ evaluation.

Loading conditions	Constant amplitude	Constant ΔK_{app}
	σ_a=23.2 MPa, R=0.1	ΔK_{app}=11 MPa$\sqrt{m}$, R=0.1

Table 2. Material constants used in the crack growth laws for 2024-T351 [19, 22]. (Unit: N, m)

Material constants	C	m	n	p	q
Walker eq.	4.8×10^{-11}	0.6937	3.2		
Forman eq.	2.864×10^{-10}	4.067			
NASGRO eq.	1.71×10^{-10}		3.353	0.5	1

Table 3. Loading conditions of fatigue tests for CT$_{4PB}$ and CT$_{BM}$ specimens.

Specimen	CT$_{4PB}$-1, 2	CT$_{BM}$-1	CT$_{4PB}$-3, 4	CT$_{BM}$-2
Residual stress	Yes	No	Yes	No
K_{res}	> 0	$= 0$	< 0	$= 0$
$\Delta K_{app, const}$ (MPa$\sqrt{m}$)	10	10	10	10
$R_{eff, const}$	0.5	0.5	0.1	0.1

Table 4. Loading conditions of fatigue tests for CT$_{FSW}$ and CT$_{BM}$ specimens.

Specimen	CT$_{FSW}$-1, 2	CT$_{BM}$-3
Residual stress	Yes	No
K_{res}	from negative to positive	$= 0$
$\Delta K_{app, const}$ (MPa$\sqrt{m}$)	10	10
$R_{eff, const}$	0.5	0.5
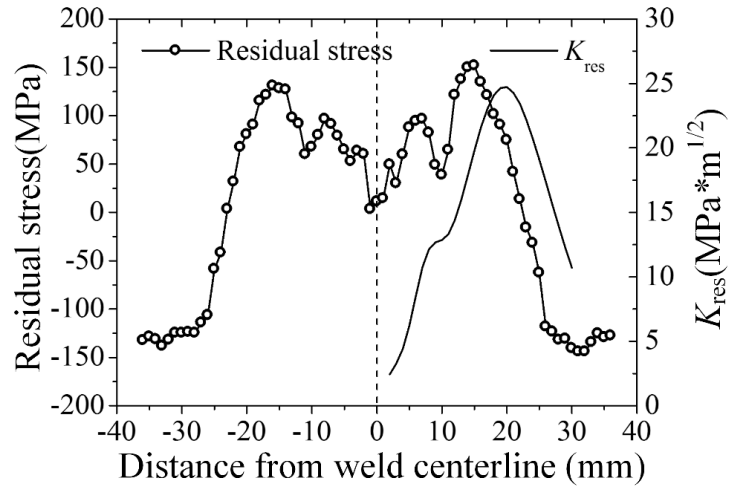
Fig. 1. Distribution of longitudinal residual stress and K_{res} of a VPPA welded specimen
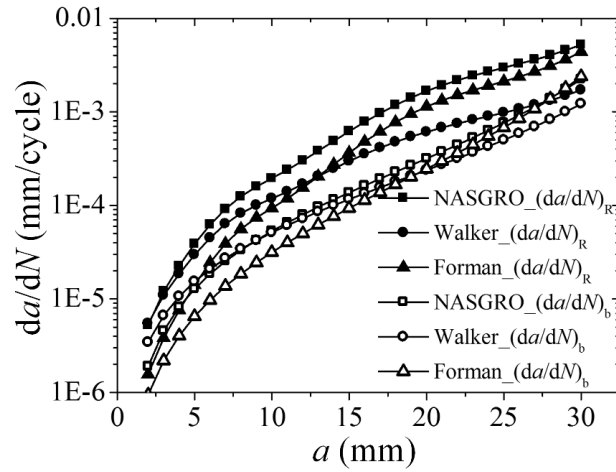
(a) Constant amplitude loading
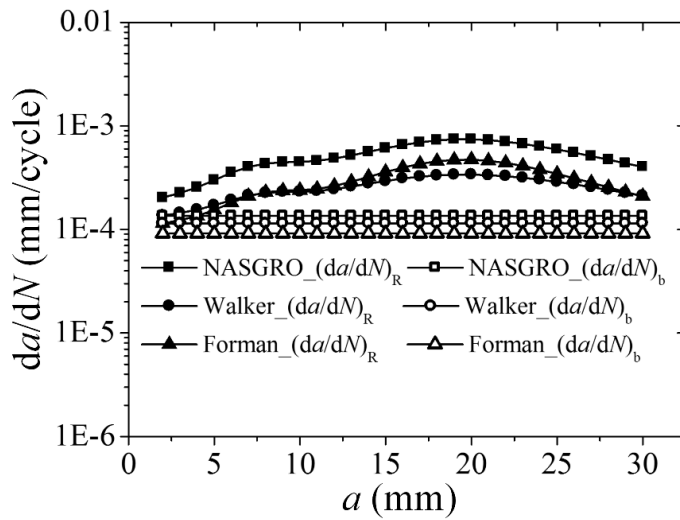
(b) Constant ΔK_{app} loading

Fig. 2. Evaluated $(da/dN)_R$ and $(da/dN)_b$ by the crack growth laws.
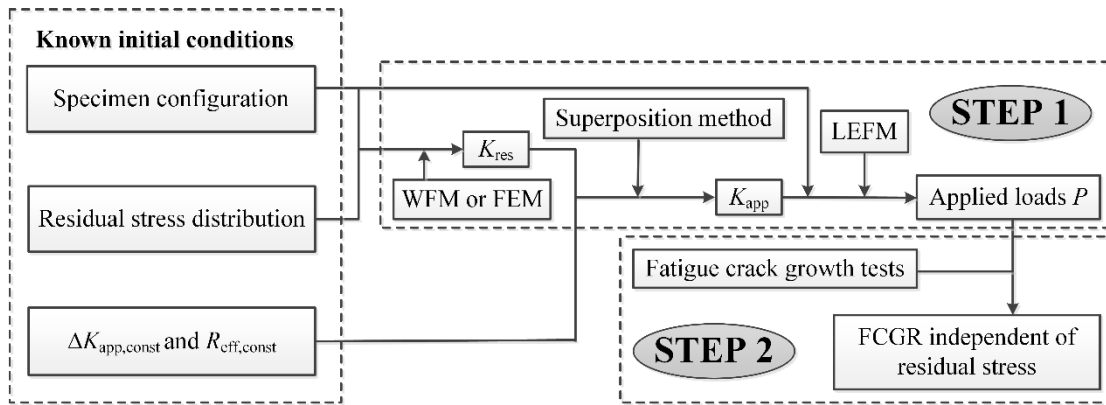
Fig. 3. Flowchart of the modified loading method and test procedure
(WFM: weight function method; FEM: finite element method)
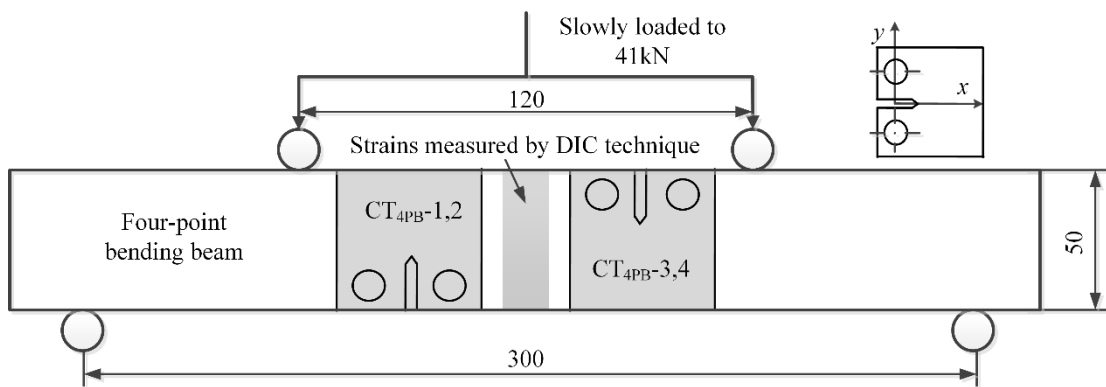
Fig. 4. Arrangement of the four-point bending test and configurations of CT$_{4PB}$ specimens
(Unit: mm. DIC, digital image correlation)
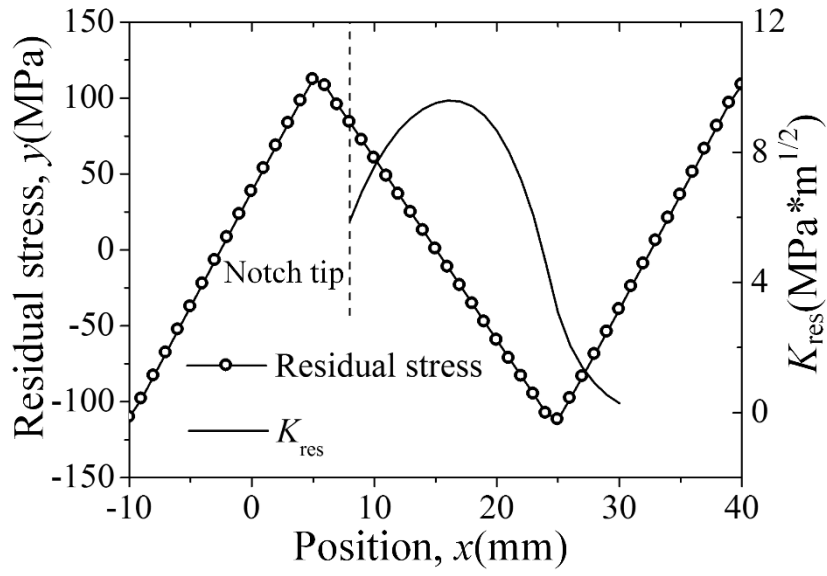
(a) CT$_{4PB}$-1, 2
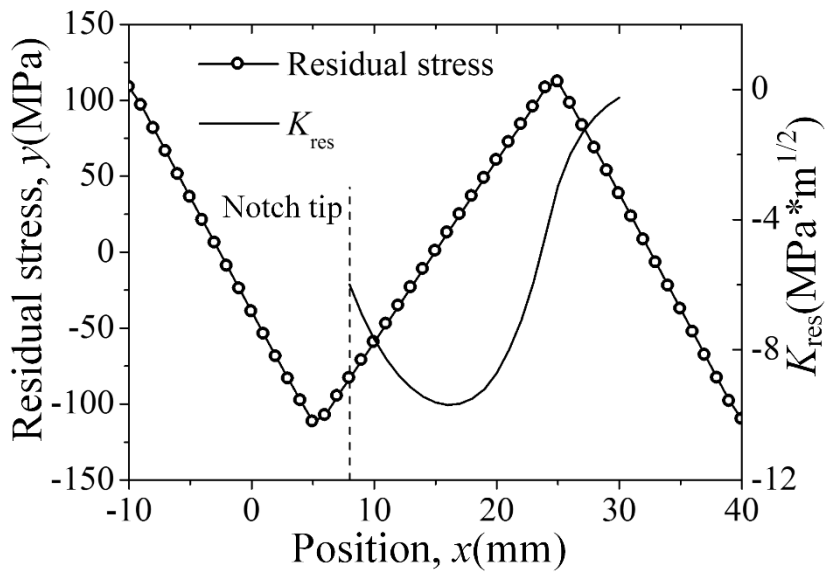
(b) CT$_{4PB}$-3, 4

Fig. 5. Distribution of residual stress and the corresponding K_{res}.
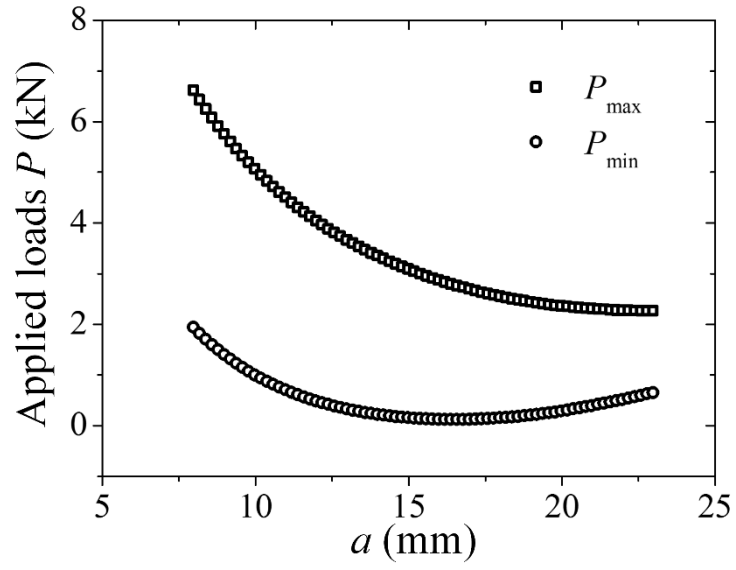
(a) CT$_{4PB}$-1, 2
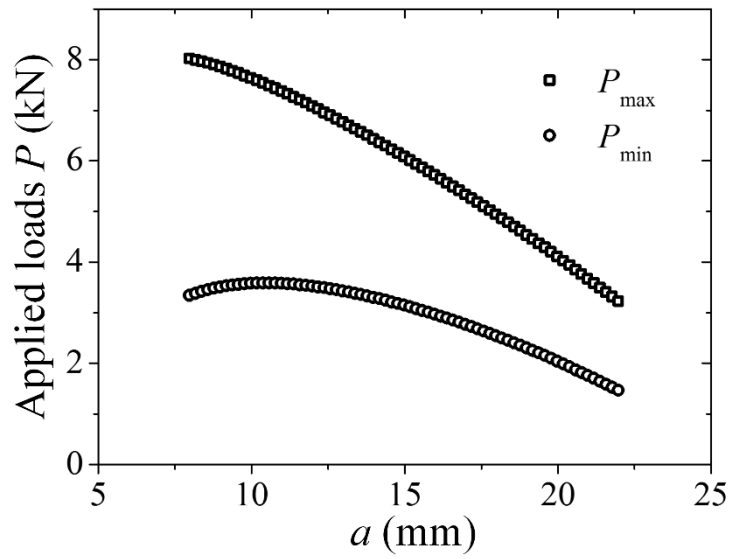
(b) CT$_{4PB}$-3, 4

Fig. 6. Changes in applied P_{max} and P_{min} to achieve constant R_{eff} and constant ΔK_{app}
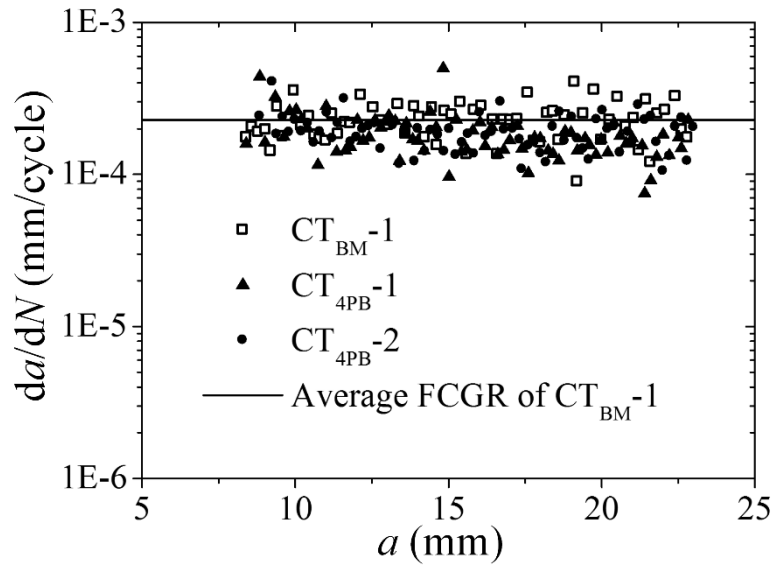
(a) CT$_{4PB}$-1, 2 and CT$_{BM}$-1
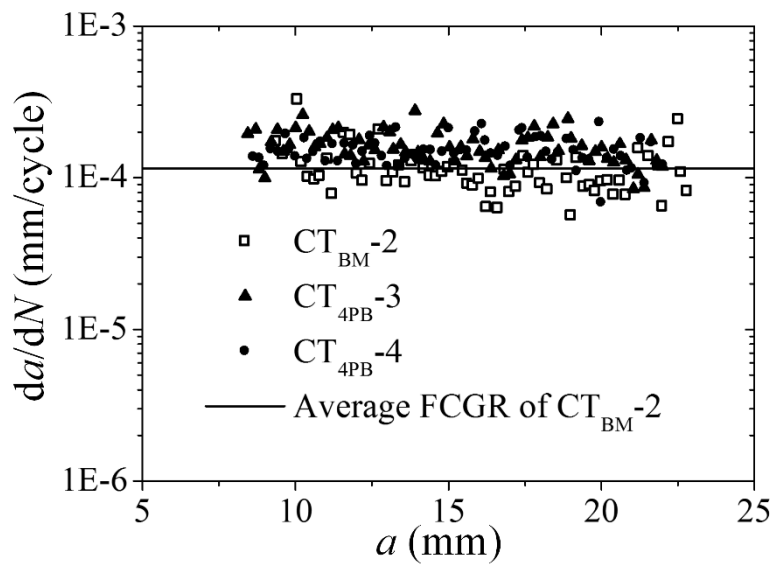
(b) CT$_{4PB}$-3, 4 and CT$_{BM}$-2

Fig. 7. Evaluated FCGRs for CT$_{4PB}$ and CT$_{BM}$ specimens.
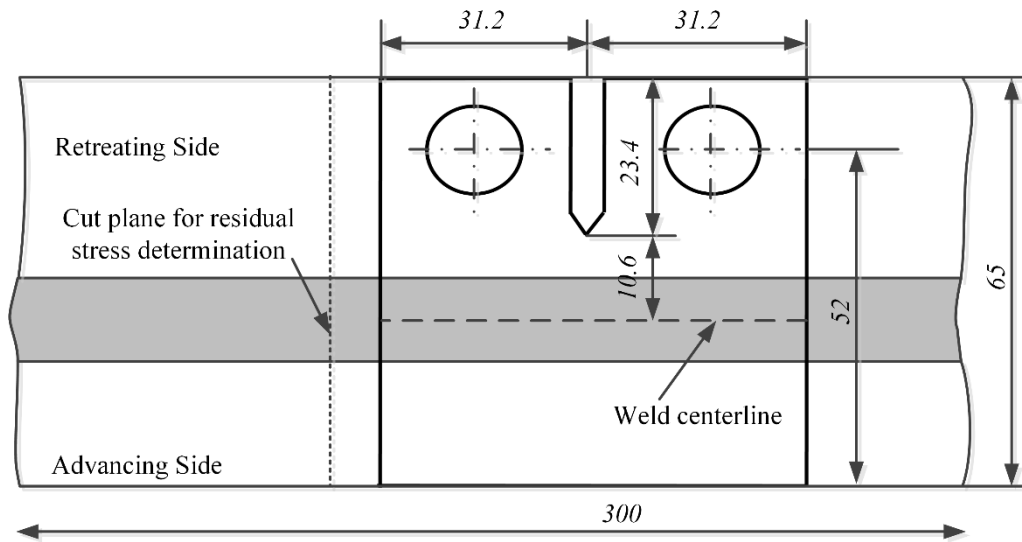
Fig. 8. Sample for residual stress determination and configuration of CT$_{FSW}$ specimens. (Unit: mm)
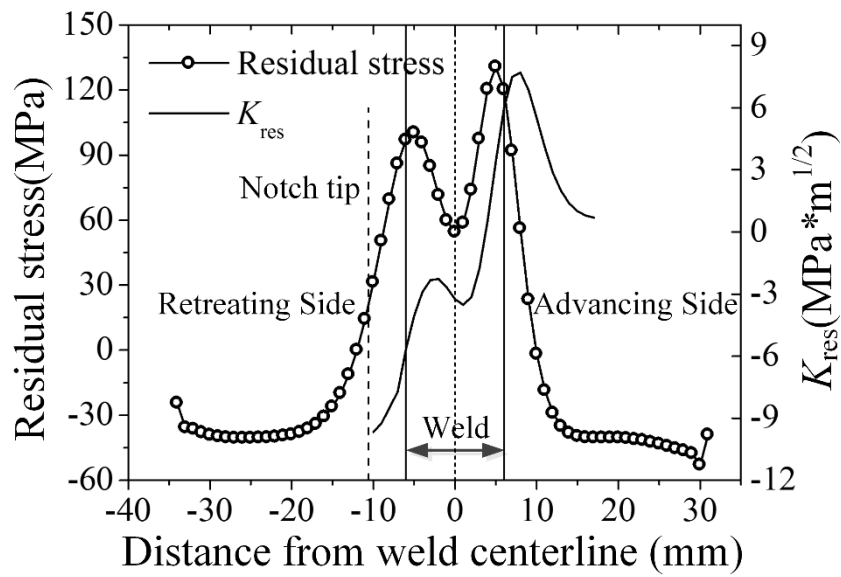
Fig. 9. Residual stress distribution and corresponding K_{res} of CT$_{FSW}$ specimens.
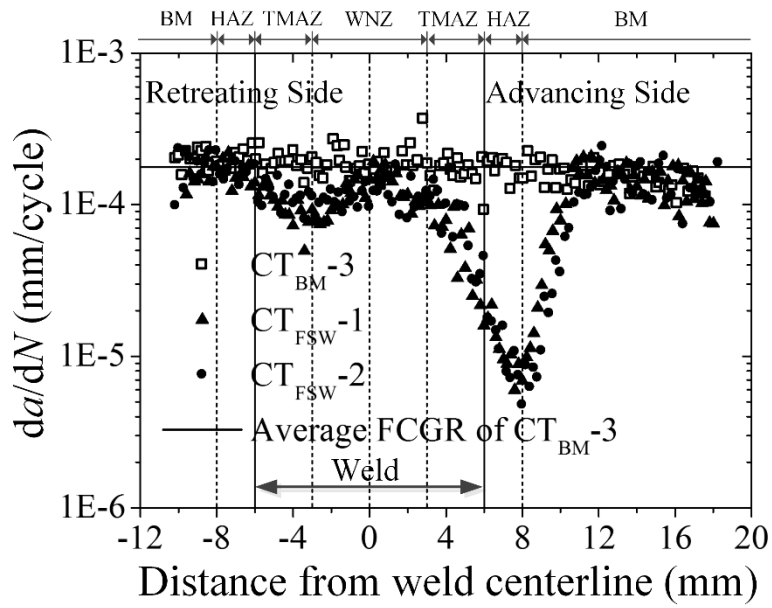
Fig. 10. Evaluated FCGRs of CT_{FSW} and CT_{BM}-3 specimens.
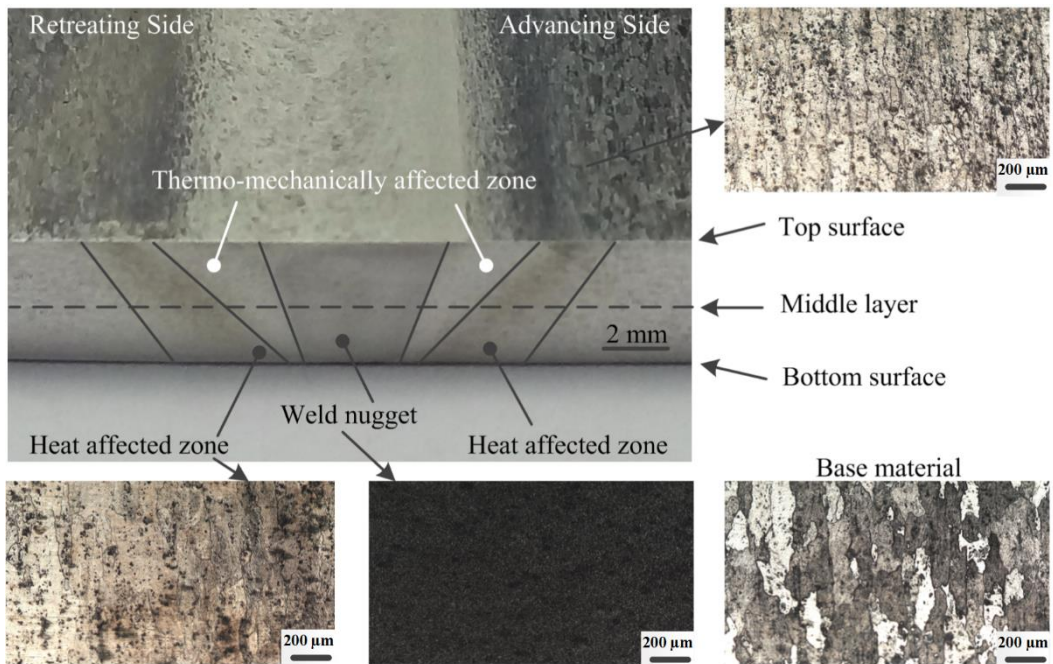
Fig. 11. Microstructure of different zones in friction stir welded 2024-T351 aluminum alloy.
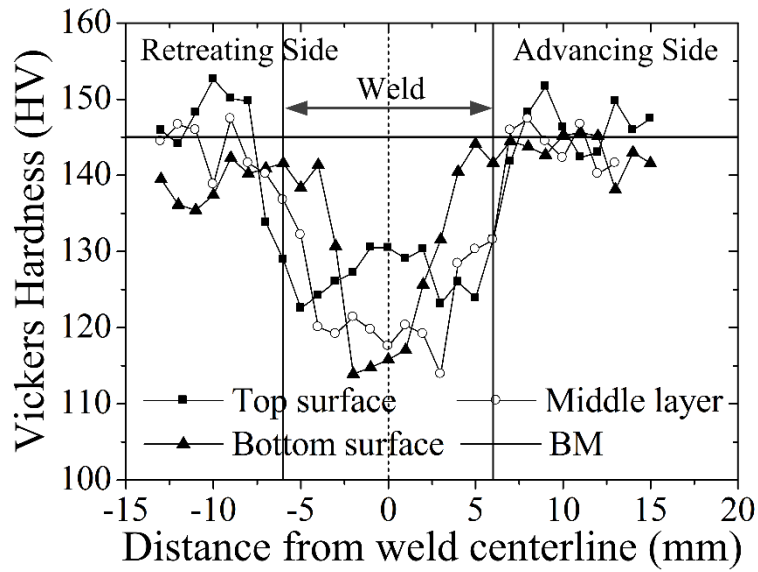
Fig. 12. Vickers hardness profiles of different layers through the thickness.
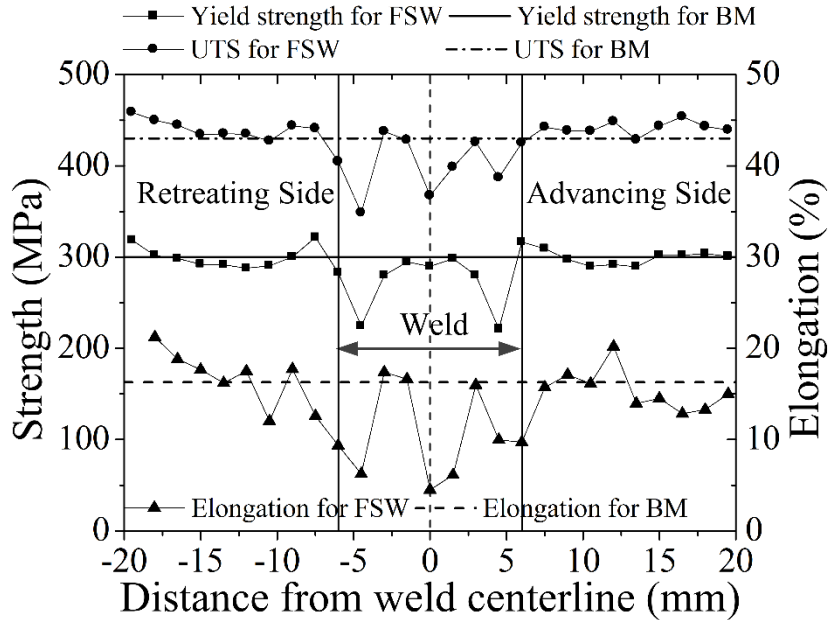
Fig. 13. Tensile properties of different weld zones and base material.